PHYSICAL REVIEW B **66**, 180402(R) (2002)

# Stripe-type charge ordering in the metallic *A*-type antiferromagnet $Pr_{0.5}Sr_{0.5}MnO_3$

R. Kajimoto,[1] H. Yoshizawa,[2] Y. Tomioka,[3] and Y. Tokura[3,4]
[1]*Department of Physics, Ochanomizu University, Bunkyo-ku, Tokyo 112-8610, Japan*
[2]*Neutron Scattering Laboratory, Institute for Solid State Physics, University of Tokyo, Tokai, Ibaraki 319-1106, Japan*
[3]*Joint Research Center for Atom Technology (JRCAT), Tsukuba, Ibaraki 305-8562, Japan*
[4]*Department of Applied Physics, University of Tokyo, Bunkyo-ku, Tokyo 113-8656, Japan*
(Received 1 October 2002; published 20 November 2002)

We demonstrate that an *A*-type antiferromagnetic (AFM) state of $Pr_{0.5}Sr_{0.5}MnO_3$ exhibits a charge ordering that governs the transport property. This charge ordering is stripelike, being characterized by a wave vector $\boldsymbol{q}\sim(0,0,0.3)$ with very anisotropic correlation parallel and perpendicular to the stripe direction. This charge ordering is specific to the manganites with relatively wide one-electron bandwidth *W* which often exhibit a *metallic A*-type AFM state, and should be strictly distinguished from the *CE*-type checkerboardlike charge ordering commonly observed in manganites with narrower *W*, such as $La_{1-x}Ca_xMnO_3$ and $Pr_{1-x}Ca_xMnO_3$.

DOI: 10.1103/PhysRevB.66.180402 PACS number(s): 75.30.Vn, 71.27.+a, 71.30.+h, 71.45.Lr

Perovskite manganites have attracted enormous interests because they exhibit a colossal magnetoresistance (CMR) effect with hole doping, where the conductivity shows a significant increase when a ferromagnetic (FM) state is induced.[1] For the most intensively studied CMR systems $Pr_{1-x}Ca_xMnO_3$ and $La_{1-x}Ca_xMnO_3$, a consensus seems to be reached concerning the mechanism of CMR. In these systems, a so-called ''*CE*-type'' charge ordering that appears at $x\sim1/2$ is considered to be an essential ingredient. A strong competition between the FM metallic region and the *CE*-type charge ordered insulating region causes a dramatic change of the transport property.

One of the important features of these compounds is that these materials have a relatively narrow one-electron bandwidth *W*, and exhibits a wide region of the *CE*-type charge ordered state on their hole concentration versus *T* phase diagrams.[2] On the other hand, the CMR phenomenon is not limited to the narrow *W* manganites, and is indeed observed in systems with wider *W* such as $Pr_{0.5}Sr_{0.5}MnO_3$,[4] $Nd_{1-x}Sr_xMnO_3$ with $x\gtrsim1/2$,[5] and $La_{2-2x}Sr_{1+2x}Mn_2O_7$ with $x=0.4$.[6] An important characteristics of these compounds is that all of them show a *highly conductive A*-type antiferromagnetic (AFM) state, and some of them even lack the *CE*-type charge ordering. To illustrate this point, we schematically depict the variation of the phase diagram as a function of *W* in Fig. 1. In contrast to a manganite with a narrow *W* (indicated by a thin dashed line), a manganite with a relatively wider *W* (a thick dashed line) generally shows a following sequence of spin/charge ordering on hole doping: insulating *A*-type AFM→*metallic* FM→*metallic A*-type AFM→insulating *C*-type, and finally insulating *G*-type AFM state. The most important feature here is a lack of the *CE*-type spin/charge ordering and the appearance of the *metallic A*-type AFM.[7,8] In the metallic *A*-type AFM, a planar orbital-ordered state with $d(x^2-y^2)$ orbitals is established around $x=1/2$.[5,9] This orbital ordering mediates the FM coupling within the orbital-ordered planes in which doped carriers possess a fairly large mobility.[5,10] At the same time, the $d(x^2-y^2)$-type orbital ordering favors the AFM coupling perpendicular to the orbital-ordered planes, and results in an overall *A*-type AFM spin state. The scenario for the CMR phenomenon based on the *CE*-type charge ordering is clearly irrelevant in this case, and another microscopic mechanism ought to be invoked.

To unravel this issue, we chose one of the cubic *A*-type AFM manganites $Pr_{0.5}Sr_{0.5}MnO_3$, and performed a detailed neutron diffraction study. $Pr_{0.5}Sr_{0.5}MnO_3$ exhibits a first-order phase transition from a FM metal to an AFM less-conductive state at $T_N\sim140$ K, accompanied with a structural transition as shown in Fig. 3(a).[4] It exhibits a significant MR ($[\rho(0)-\rho(H)]/\rho(H)]>1000\%$) below $T_N$. With a high quality single crystal sample, we found that there exists a novel stripe-type charge ordering with the modulation vector $q\sim0.3$ r.l.u. (reduced lattice units) at all *T*. In what follows, we shall demonstrate that the quasistripe order is intrinsic to the planar $d(x^2-y^2)$-type orbital ordering, and the transport property in the *metallic A*-type AFM is, in fact, controlled by the stripe-type charge ordering. The present results provide strong evidence that the physics of the CMR phenomena in the *A*-type AFM manganites is fundamentally different from the narrow *W* manganites where the *CE*-type charge ordering plays a crucial role.

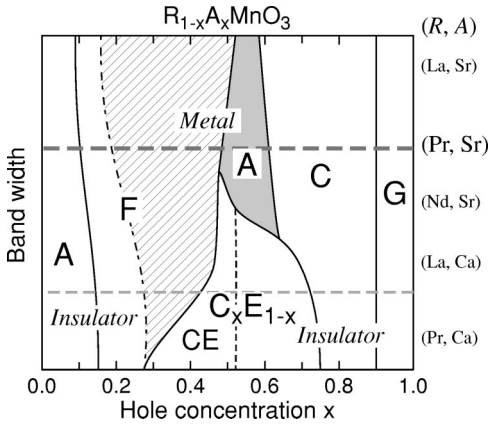


FIG. 1. Schematic phase diagram of $R_{1-x}A_xMnO_3$. *F* denotes FM state. *A*, *CE*, *C*, and *G* denote *A*-type, *CE*-type, *C*-type, and *G*-type AFM states, respectively. $C_xE_{1-x}$ represents incommensurate charge/orbital ordered state (Ref. 2).

 

The single-crystal sample well characterized in the preceding studies[4,10,11] was reinvestigated by neutron diffraction technique. An incident neutron momentum $k_i = 3.83$ Å$^{-1}$ and a combination of 40′-40′-40′-80′ collimators were utilized at the triple-axis spectrometer GPTAS installed at the JRR-3M reactor in JAERI, Tokai, Japan. Two pyrolytic graphite filters were placed before and after the sample to suppress higher-order contaminations. The sample was mounted in an Al can filled with He gas, and was attached to the cold head of a closed-cycle helium gas refrigerator. The temperature was controlled within an accuracy of 0.2 K.

The crystal structure of $Pr_{0.5}Sr_{0.5}MnO_3$ is tetragonal $I4/mcm$ with $a=b\sim5.4$ Å and $c/\sqrt{2}\sim5.5$ Å in the paramagnetic (PM) and FM states and monoclinic $P2_1/n$ with $a\sim c\sim5.4$ Å, $b/\sqrt{2}\sim5.5$ Å, and $\beta\sim91°$ in the AFM state.[10,12] For simplicity, we employ the cubic notation with $a\sim3.8$ Å, so that the FM layers of the *A*-type AFM structure are perpendicular to the [010] direction. All the diffraction measurements were carried out on the $(h,0,l)$ scattering plane to measure the correlations within the FM layers in the *A*-type AFM states.

To examine whether $Pr_{0.5}Sr_{0.5}MnO_3$ exhibits a charge ordering, we surveyed the $(h,0,l)$ scattering plane at selected $T$'s. Figure 2 presents maps of the scattering intensities collected around (0,0,2) in the *A*-type AFM phase at $T=7$ K, in the FM phase at 180 K, and in the PM phase at 275 K. The intense fundamental nuclear Bragg reflection was observed at (0,0,2). At 7 K, *A*-type AFM Bragg reflections are observed at $(\pm0.5,0,2)$. Two ring-shaped scatterings observed at all $T$'s are powder scattering from the Al sample cell. In addition, twinning and mosaic distributions of the crystal yield a nuclear reflection near $(-0.1,0,2)$ as well as an *A*-type AFM Bragg reflection near (0,0,1.6), but they were slightly displaced from the commensurate positions due to the small deviations of the lattice constants of respective domains from the ideal cubic symmetry. We also observed the weak *CE*-type superlattice reflections appearing at $\boldsymbol{Q}\sim(\pm0.2,0,2.2)$ in the AFM phase [Fig. 2(a)]. In the present case, however, the *CE*-type ordered region has practically no influence on the transport property, because its volume fraction is negligibly small. It is estimated as ~1% by the intensities of the *CE*-type AFM peaks. We note that the coexistence of the *A*-type metallic AFM region and the parasitic *CE*-type insulating region was frequently observed in the manganites with $x\sim1/2$.[9,13,14]

The important results in Fig. 2 are anisotropic diffuse scatterings indicated by white arrows. They are centered at $\boldsymbol{Q}\sim(0,0,2\pm0.3)$, and are elongated towards the [100] direction. The anisotropy of their profiles indicates that the correlation length along $\boldsymbol{q}=(0,0,\pm0.3)$ ($\xi_\parallel$) is much longer than that perpendicular to $\boldsymbol{q}$ ($\xi_\perp$). By deconvoluting the insturumental resolutions, the inverse correlation lengths are determined as $\kappa_\parallel\sim0.02$ r.l.u. and $\kappa_\perp\sim0.24$ r.l.u. at 7 K. Although the diffuse scattering becomes weaker in the FM and PM states, it remains finite, but the positions of the signals shift slightly towards $\boldsymbol{Q}\sim(0,0,2\pm0.25)$. Because the similar scatterings are observed at large $Q$ but less clear at small $Q$, the origin of the scatterings is attributable to lattice modulations. Due to the twinning domains with propaga-

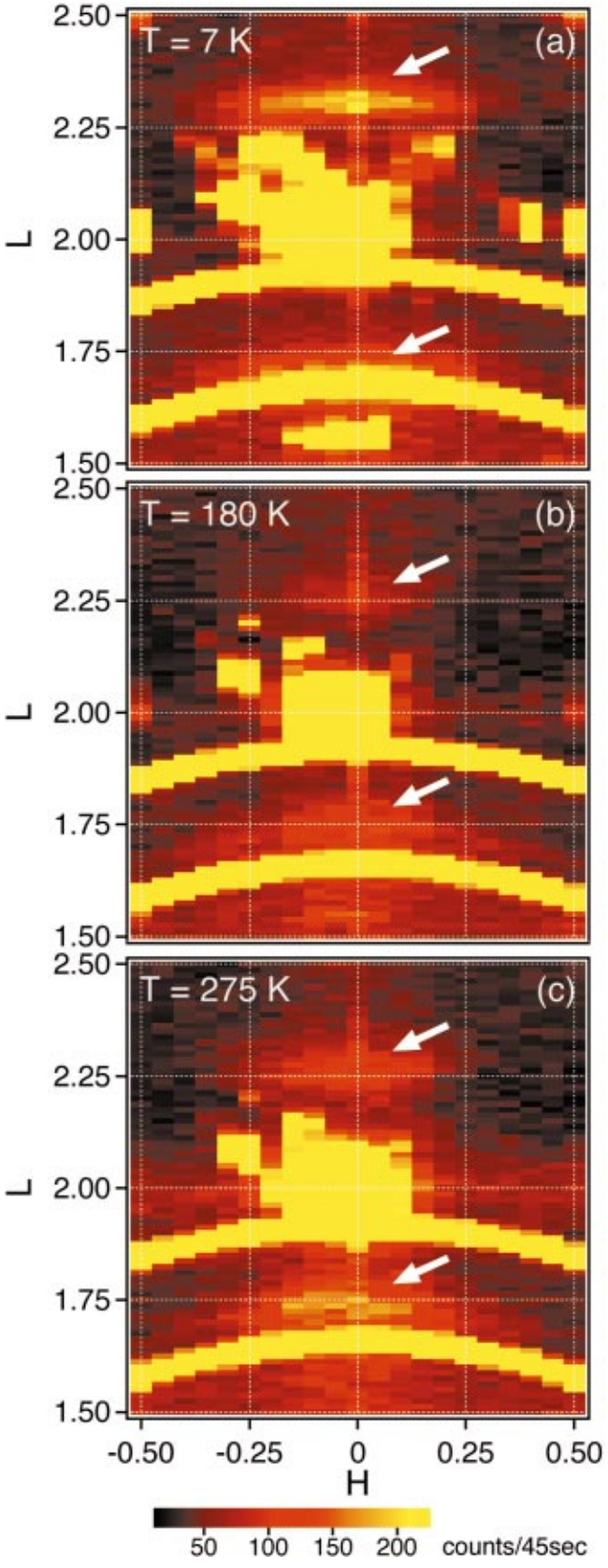


FIG. 2. (Color) Intensity maps around (0,0,2) at (a) $T=7$ K, (b) 180 K, and (c) 275 K. Two ring-shaped scatterings observed at all temperatures are due to the Al sample cell. At 7 K, *A*-type AFM Bragg reflections are observed at $(\pm0.5,0,2)$.

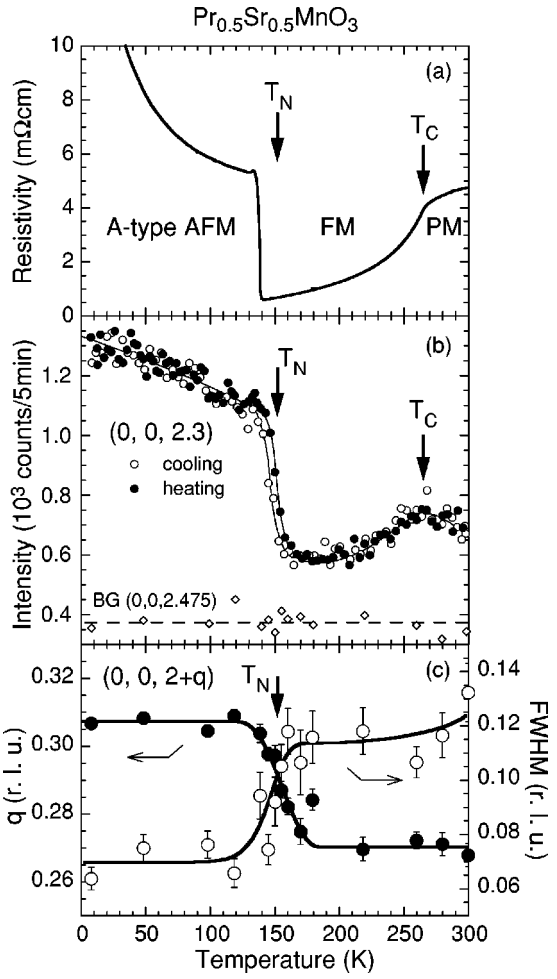


FIG. 3. (a) Temperature dependence of the resistivity. (b) Temperature dependence of the intensity at (0,0,2.3). The background intensity measured at (0,0,2.475) is also shown. Open symbols and closed symbols denote the data for cooling and for heating, respectively. (c) Temperature dependence of the wave vector (closed symbols) and the peak width or FWHM (open symbols) of the charge order peak (0,0,2.3).

tion vectors $\boldsymbol{q}=(0,0,0.3)$ or (0.3,0,0), similar scattering is expected at $(\pm 0.3,0,2)$ in Fig. 2(a), but we found no signal at corresponding positions. This suggests that the lattice modulations consist of a longitudinal component because the scattering cross section has a term $|\boldsymbol{Q}\cdot\boldsymbol{\eta}|^2$, where $\boldsymbol{\eta}$ represents a displacement vector of constituent ions. A similar feature was also observed in the stripelike charge ordering in a two-dimensional (2D) *A*-type AFM manganite $La_{2-2x}Sr_{1+2x}Mn_2O_7$.[15,16]

In order to confirm that the diffuse scattering comes from the charge ordering, its influence on the transport property was examined by the *T* dependences of the intensity, the peak width, and the wave vector of the diffuse scattering. We found a strong correlation between the resistivity and these quantities, which establishes that the observed diffuse scattering indeed arises from the charge ordering. In Figs. 3(a) and Fig. 3(b) are plotted the *T* dependences of the resistivity and that of the diffuse intensity at (0,0,2.3), respectively. Figure 3(c) shows the *T* dependence of the peak position (the

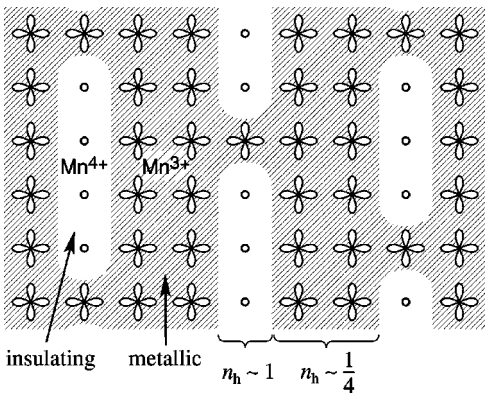


FIG. 4. Schematic illustration of the charge order and orbital order with $q=1/3$ r.l.u. Cloverleaf symbols represent the $d(x^2-y^2)$ orbitals. $n_h$ denotes the hole concentration within the $Mn^{4+}$ stripe or the $Mn^{3+}$-like matrix.

modulation wave vector) and the peak width [full width at half maximum (FWHM)] measured along the longitudinal direction (parallel to the modulation vector). In the *A*-type AFM state for $T<T_N$, the correlation of the charge ordering is well developed. The diffuse peak has large intensity, and its width is quite sharp, although it is much broader than the instrumental resolution ($\sim$0.03 r.l.u.). In this phase, the resistivity exhibits a steep increase with lowering *T*. At $T_N$, the system undergoes a first-order transition. The intensity of the charge ordering and the resistivity show sudden decreases at $T_N$. In addition, the correlation length of the charge ordering decreases, while its peak position shifts to a smaller wave vector on crossing $T_N$. Upon raising *T*, however, the intensity of the charge ordering gradually increases, and the resistivity recovers the metallic behavior. Around $T_C$, the resistivity as well as the intensity of the charge ordering shows a cusp and enters the PM state. Note that the diffuse scattering subsists in the FM as well as PM states in $Pr_{0.5}Sr_{0.5}MnO_3$.

The development of charge ordering in the *A*-type AFM phase clearly indicates that this charge ordering is intrinsic to the *A*-type AFM state with $d(x^2-y^2)$ orbital ordering. The existence of weak signals of the charge ordering in the FM and PM states implies the influence of the orbital ordering in these states, which is consistent with our previous reports.[11] Since a similar charge ordering was observed in the 2D *A*-type AFM manganites, the existence of such charge ordering must be independent to the spatial dimensionality of the manganites, and is one of the key features of the wide *W* manganites that are accompanied with the $d(x^2-y^2)$-*type orbital ordering*.

The observed charge ordering has some distinct features. First of all, the amplitude of the wave vector $q\sim 0.3$ r.l.u. is far apart from its nominal hole concentration $x=1/2$. Second, the correlation length perpendicular to the propagation vector $\boldsymbol{q}$ ($\xi_\perp$) is much shorter than that parallel to $\boldsymbol{q}$ ($\xi_\parallel$), as shown in Fig. 2. A model of the stripelike charge ordering depicted in Fig. 4 for $q=1/3$ r.l.u. provides the simplest explanation for these features. In this model, $Mn^{4+}$ ions segregate within the metallic matrix of $Mn^{3+}$-like sites with $d(x^2-y^2)$ orbitals and form stripelike objects along the Mn-

O-Mn bond direction. The $Mn^{4+}$ stripes are insulating, and they block the hopping of the $e_g$ electrons. On the other hand, the $e_g$ electrons can be mobile in the $Mn^{3+}$-like matrix, which is in stark contrast to the insulating *CE*-type charge ordering. Thus, the charge-ordered *A*-type AFM state can retain high conductivity. In Fig. 4, the hole concentration of the $Mn^{4+}$ stripe is fixed to 1, while that of two $Mn^{3+}$ lines be 1/4, resulting in the overall concentration $x=1/2$. In reality, some $e_g$ electrons may enter the line of $Mn^{4+}$ ions as depicted in Fig. 4, causing the deviation of the hole density within stripes to be $<1$, while that of the $Mn^{3+}$-like matrix regions to be $>1/4$, respectively. The excess electrons in the $Mn^{4+}$ lines will intervene the correlation along the stripes resulting in the observed anisotropy in the correlation lengths, $\xi_\perp < \xi_\parallel$.

The large discrepancy between the hole concentration and the amplitude of the wave vector is also observed in 2D manganites $La_{2-2x}Sr_{1+2x}Mn_2O_7$. In this system, the wave vector is effectively fixed at $q \sim 1/3$ for a wide region of the hole concentration.[15] A fixed wave vector can be explained by the model in Fig. 4 as the tuning of the overall hole concentration by introducing excess electrons or holes within the stripes and the $Mn^{3+}$-like matrix regions. It should be noted that the wave vector of the charge ordering in $Pr_{0.5}Sr_{0.5}MnO_3$ slightly shifts through the transition from the *A*-type AFM state to the FM state as seen in Fig. 3(c). This behavior indicates that the mechanism of the formation of the stripe-type charge ordering is susceptible to the change of the spin/orbital structure and the concomitant change of the electronic state.

Another important feature of the present stripelike charge ordering is that the charge stripes are parallel to the Mn-O bonds in contrast to the *CE*- and $C_xE_{1-x}$-type charge ordering.[17] The direction of the stripes may be a consequence of the large mobility due to the wide *W* and the 2D orbital ordering in the *A*-type AFM state. The double exchange (DE) mechanism mediated by the hopping of holes is a leading interaction within the metallic orbital-ordered planes, while the superexchange (SE) interactions are dominant within stripes and at the boundaries between $Mn^{4+}$ stripes and metallic regions. In the case of the ''parallel'' charge order, the number of the Mn-O-Mn bonds mediating the DE interactions is much larger than that in the case of the ''diagonal'' charge order. When *W* is sufficiently large, the DE interaction overwhelms the SE interaction, and the parallel charge order is favored by maximizing the number of the DE bonds. On the contrary, when *W* is small, the SE interactions dominate and favor the diagonal charge order known as the *CE*-type and $C_xE_{1-x}$-type.[18]

A similar relation between the charge mobility and the direction of stripes holds in the well-known stripe ordered systems, i.e., high-$T_c$ cuprates.[19] This implies that there is a common origin of the stripe order underlying these systems. We would like to point out that the $d(x^2-y^2)$ orbital state is common to both *A*-type AFM manganites and high-$T_c$ cuprates: the *metallic* transition metal oxides with $d(x^2-y^2)$ orbitals may involve an instability to the formation of the parallel charge stripe.

To summarize, a neutron diffraction study was performed on a single crystal of $Pr_{0.5}Sr_{0.5}MnO_3$. We found an anisotropic charge ordering with a wave vector $\boldsymbol{q} \sim (0,0,0.3)$. The character of the charge ordering is consistent with the stripe-like charge ordering. This charge ordering exists in the manganites with a wide one-electron bandwidth and with the $d(x^2-y^2)$-type orbital ordering regardless of its spatial dimensionality. The CMR phenomenon in these materials must be understood on the basis of this ''*stripe-like charge ordering*.''

We thank H. Kawano-Furukawa for valuable discussions. This work was supported by a Grant-In-Aid for Scientific Research from MEXT, Japan, and by NEDO of Japan.

[1] M. Imada, A. Fujimori, and Y. Tokura, Rev. Mod. Phys. **70**, 1039 (1998).

[2] The incommensurate charge and orbital order observed at $x > 1/2$ (Ref. 17) can be regarded as an extension of the *CE*-type charge/orbital order, and we represent it by $C_xE_{1-x}$ in Fig. 1 following Ref. 3.

[3] E. Dagotto, T. Hotta, and A. Moreo, Phys. Rep. **344**, 1 (2001).

[4] Y. Tomioka *et al.*, Phys. Rev. Lett. **74**, 5108 (1995).

[5] H. Kuwahara *et al.*, Phys. Rev. Lett. **82**, 4316 (1999).

[6] Y. Moritomo *et al.*, Nature (London) **380**, 141 (1996).

[7] Y. Moritomo *et al.*, Phys. Rev. B **55**, 7549 (1997).

[8] T. Akimoto *et al.*, Phys. Rev. B **57**, R5594 (1998).

[9] R. Kajimoto *et al.*, Phys. Rev. B **60**, 9506 (1999).

[10] H. Kawano *et al.*, Phys. Rev. Lett. **78**, 4253 (1997).

[11] H. Kawano *et al.*, cond-mat/9808286 (unpublished); H. Yoshizawa *et al.*, Mater. Sci. Eng., B **B63**, 125 (1999); R. Kajimoto *et al.*, J. Magn. Magn. Mater. **226-230**, 892 (2001).

[12] A. Llobet *et al.*, Phys. Rev. B **60**, R9889 (1999).

[13] Y. Moritomo *et al.*, Phys. Rev. B **58**, 5544 (1998).

[14] M. Kubota *et al.*, J. Phys. Soc. Jpn. **68**, 2202 (1999).

[15] M. Kubota *et al.*, J. Phys. Soc. Jpn. **69**, 1986 (2000).

[16] L. Vasiliu-Doloc *et al.*, Phys. Rev. Lett. **83**, 4393 (1999).

[17] S. Mori, C.H. Chen, and S-W. Cheong, Nature (London) **392**, 473 (1998); P.G. Radaelli *et al.*, Phys. Rev. B **59**, 14 440 (1999).

[18] For a related discussion, see T. Mizokawa, and A. Fujimori, Phys. Rev. Lett. **80**, 1320 (1998).

[19] J.M. Tranquada *et al.*, Nature (London) **375**, 561 (1995).